IEEE TRANSACTIONS ON
SMART GRID

Flexibility Reserve in Power Systems: Definition and Stochastic Multi-Fidelity Optimization

Roohallah Khatami, *Student Member, IEEE*, Masood Parvania, *Senior Member, IEEE*, and Akil Narayan

***Abstract*—This paper defines flexibility reserve trajectory as a single reserve product that not only supplies the energy imbalance in real-time operation but also the resulting ramping requirements by embedding the flexible ramping trajectories as time derivative of the reserve trajectories. Further, a stochastic optimization model is proposed for multi-fidelity co-optimization of energy and flexibility reserve in day-ahead power systems operation. The proposed model integrates operation decisions with different levels of modeling fidelity in a single stochastic optimization problem. More specifically, day-ahead energy trajectories, day-ahead flexibility reserve capacity trajectories, and real-time flexibility reserve deployment trajectories are modeled by Bernstein polynomials with different degrees as required to match the load and renewable generation with different levels of variability in day-ahead and real-time operations. The proposed model is implemented on the IEEE reliability test system using load and solar generation data of California ISO, where the numerical results demonstrate that the proposed model schedules a reserve capacity that more accurately matches the real-time energy imbalance and ramping requirements of net-load, while reducing the total operation cost of the system.**

***Index Terms*—Continuous-time unit commitment, stochastic optimization, flexibility reserve, uncertainty characterization, mixed integer linear programming.**

I. Introduction

LARGE-scale integration of intermittent renewable energy sources (RES) is calling for additional flexibility resources as well as more advanced modeling and optimization techniques to account for the increasing uncertainty and variability in power systems operation [1]. As the RES integration gains momentum, the magnitude and frequency of their variations increase, which may trigger ramping scarcity events in real-time power systems operation [2]–[4]. This necessitates revisiting the present definition of power systems flexibility and reserve services in order to reflect their robustness and adequacy towards sub-interval variations of the load and RES, as well as adjusting the operation models to accomodate the new reserve services [2]–[5].

Multiple research works have been conducted on developing models for evaluating flexibility of power systems. A probabilistic metric, called insufficient ramping resource expectation, is developed in [6], [7] for evaluating the flexibility of power systems. A statistical analysis is conducted in [8] to evaluate the flexibility requirement of power systems in European power systems, where the flexibility is defined based on the magnitude and frequency of ramping events of net-load (load minus renewable generation). In [9], a deterministic multi-time-scale day-ahead scheduling model is proposed that enables co-optimizing the energy and ancillary services, with sub-hourly flexible ramping products. In [10], look-ahead security-constrained unified unit commitment and economic dispatch models are formulated to tap the flexibility resources in case of contingency events, where each receding horizon embeds four sets of time intervals with different resolutions.

In addition, there has been significant advancement in the application of stochastic optimization models for reserve and flexibility scheduling in power systems operation [11]–[13]. A security constrained unit commitment (UC) model is developed in [14] that takes into account the intermittency and volatility of wind power generation in day-ahead scheduling decisions. In [15], spinning and non-spinning reserve requirements are evaluated for a power system with uncertain wind power output, and metrics are calculated to evaluate the cost saving due to utilization of wind power and the cost incurred due to reserve deployment when the wind power output does not meet the scheduled level. A two-stage stochastic UC model is proposed in [16] that utilizes the operating reserve provided by flexible loads to enhance the operational security of bulk power systems. A stochastic UC model is proposed in [17] where the day-ahead energy schedule of the thermal generating units, flexible loads, and ES devices are co-optimized with the flexible ramping offered by thermal units. In [18], a two-stage stochastic optimization model is proposed to explore the potential capability of wind units in providing flexible ramping services, including the real-time UC and economic dispatch as first and second stages. A chance-constrained stochastic UC model is proposed in [19] for scheduling reserve to supply the expected net-load uncertainties.

Although different in problem formulation and solution techniques, the stochastic flexibility scheduling models in literature utilize the same discrete-time piecewise constant trajectories for modeling the decisions in day-ahead scheduling and real-time realization stages. However, in reality, the real-time reserve deployment decisions are taken in faster pace than the day-ahead scheduling decisions (e.g., 5-min real-time decisions versus hourly day-ahead schedules). Therefore, approximating the real-time operation decisions with the same modeling accuracy of the day-ahead decisions in stochastic UC models prevents capturing faster real-time net-load variations and reserving adequate generation capacity to compensate the variation [4], which may trigger ramping scarctiy events and necessitate scheduling flexible ramping products in real-time

This work was supported by U.S. Department of Energy under Grant DE-OE0000882. R. Khatami and M. Parvania are with the Department of Electrical and Computer Engineering, University of Utah, Salt Lake City, UT 84112 USA (e-mails: {roohallah.khatami, masood.parvania}@utah.edu). A. Narayan is with the Department of Mathematics, University of Utah, Salt Lake City, UT 84112 (e-mail: {akil@sci.utah.edu)

Digital Object Identifier: 10.1109/TSG.2019.2927600

operation, as experienced by few system operators [2], [3].

A. Contribution

This paper proposes a novel stochastic optimization model for multi-fidelity scheduling of energy and flexibility reserve capacity in day-ahead operation. The proposed model, formulated as a two-stage stochastic optimization problem, co-optimizes day-ahead decision trajectories in the first stage with higher-fidelity real-time decision trajectories in the second stage. The term *fidelity* refers to the modeling accuracy of parameters and decision trajectories in the optimization problem. The proposed multi-fidelity modeling approach enables integrating and optimizing different decision trajectories with different levels of accuracy in a single optimization problem [20]. The major contributions of this paper include:

- This paper defines *flexibility reserve trajectory* that combines the balancing reserve and flexible ramping products in current markets, as it embeds *flexible ramping trajectories* as time derivative of the reserve trajectories. Thus, the flexibility reserve not only supplies the real-time energy imbalance, but also the real-time ramping requirements by a single reserve product.
- The variability and uncertainty of load and RES are characterized by continuous-time stochastic processes. A second-order moment matching method is proposed to reduce the dimensionality of continuous probability spaces and Bernstein polynomials of different degrees are used to model the day-ahead mean and real-time realizations with different fidelity.
- The proposed model integrates decisions with different levels of fidelity in a single stochastic optimization problem: day-ahead energy trajectories, day-ahead flexibility reserve capacity trajectories, and real-time flexibility reserve deployment trajectories are modeled with Bernstein polynomials with three different degrees as required to match the variability and uncertainty of load and RES in day-ahead and real-time operations. The proposed model includes as a special case the current discrete-time stochastic UC model by choosing Bernstein polynomials of degree 0 for modeling all decision variables.

The proposed stochastic optimization model is formulated in Section II, where the decision variable are modeled as continuous-time trajectories. In Section III, Bernstein polynomials are utilized to model load and RES generation with different fidelity over time, and a second-order moment matching method is proposed to reduce the probability space dimensionality of the processes. Using the models in Section III, the multi-fidelity stochastic optimization model is formulated in Section IV as a mixed-integer linear programming (MILP) problem. The numerical results, conducted on the IEEE-RTS using California ISO load and solar generation, are presented in Section V, and the conclusions are drawn in Section VI.

B. Notation

The following notation is used throughout the paper: boldface letters indicate the matrices and vectors. The subscripts k, j, q, n, and ω respectively represent the indexes of generating units, time intervals, Bernstein polynomials covering a single time interval, lineariztion segments of the cost function, and net-load realizations. The superscripts u and d respectively represent the up and down flexibility reserve. The letters G, R, I, r, D, G^R, N, SP respectively represent the day-ahead generation, flexibility reserve capacity, and commitment status of generating units, real-time flexibility reserve deployment of generating units, load, renewable generation, net-load, and renewable spillage. The dots over decision variables, i.e., $\dot{G}$, $\dot{I}$, and $\dot{r}$ represent their time-derivatives. The overlined and underlined letters respectively represent the upper and lower limits of trajectories. The continuous time is t, a specific time is t_j, $T_j = t_{j+1} - t_j$ and scheduling horizon is represented by $\mathcal{T}$. The letters Ω, $\mathcal{F}$, and $\mathbb{P}$ together form the probability space of stochastic processes and respectively represent the sample space, set of events, and probability measure. The superscripts d and g distinguish the probability spaces of load and renewable generation.

II. The Proposed Stochastic Optimization Model

1) Characterizing the Uncertainty of Load and Solar Generation: Let the total load and non-dispatchable renewable generation be independent continuous-time stochastic processes, respectively shown by $D(t)$ and $G^R(t)$, and defined over probability spaces $(\Omega^d, \mathcal{F}^d, \mathbb{P}^d)$ and $(\Omega^g, \mathcal{F}^g, \mathbb{P}^g)$. Let us also represent the realizations of such processes with $d_\omega(t)$ and $g^R_\omega(t)$, where ω is an event in either Ω^d or Ω^g, and $t \in \mathcal{T}$. Further, let us define a stochastic process $N(t) = (D(t), G^R(t))$ as the concatenation of load and renewable generation processes, where $n_\omega(t) = (d_\omega(t), g^R_\omega(t))$ is a realization of the process. Formally, this process can be associated to a new probability space $(\Omega, \mathcal{F}, \mathbb{P})$, where $\Omega = \Omega^d \times \Omega^g$, $\mathcal{F} = \mathcal{F}^g \otimes \mathcal{F}^d$, and $\mathbb{P}$ is the product measure formed from $\mathbb{P}^d$ and $\mathbb{P}^g$. We assume hereafter that all stochastic quantities, denoted with or dependent on ω, are members of the probability space $(\Omega, \mathcal{F}, \mathbb{P})$.

This paper characterizes the probability spaces of load and renewable generation by continuous-time Gaussian processes, i.e., $D(t) \sim \mathcal{GP}\left(D_0(t), c^d(t,t')\right)$ and $G^R(t) \sim \mathcal{GP}\left(G^R_0(t), c^g(t,t')\right)$, where $D_0(t)$ and $G^R_0(t)$ are the mean, and $c^d(t,t')$ and $c^g(t,t')$ represent the covariance functions of the processes. Therefore, the net-load process $N(t)$ is also a Gaussian process, i.e., $N(t) \sim \mathcal{GP}\left(N_0(t), c^n(t,t')\right)$, where $N_0(t)$ and $c^n(t,t')$ are the mean and covariance functions. Gaussian process with customized covariance function is shown to be effective to model load and renewable power generation (see e.g., [21]–[24]).

2) Modeling Generating Units: Assume that a set of K generating units are available to supply the net-load over the scheduling horizon $\mathcal{T}$. We model generating units by vector of positive day-ahead generation trajectories $\mathbf{G}(t) = \left(G_1(t), \ldots, G_K(t)\right)^T$, along with day-ahead commitment statuses $\mathbf{I}(t) = \left(I_1(t), \ldots, I_K(t)\right)^T$, and ramping trajectories $\dot{\mathbf{G}}(t) = \left(\dot{G}_1(t), \ldots, \dot{G}_K(t)\right)^T$ that are defined as time derivatives of the generation trajectories. The day-ahead generation cost of generating unit k is shown by $C\left(G_k(t)\right)$. In addition, vectors $\mathbf{SU}(t)$ and $\mathbf{SD}(t)$ show the startup and shutdown cost variables of units.

3) Modeling Flexibility Reserve and Flexible Ramping: this paper defines *up and down flexibility reserves* as the reserve trajectories that are provided by generating units to compensate the variability and uncertainty of net-load trajectory in power systems operation. The up and down flexibility reserves are characterized by the day-ahead capacity and real-time deployment trajectories. The *day-ahead capacity trajectories* of up and down flexibility reserves are respectively represented by vectors of positive variables $\mathbf{R}^u(t) = (R_1^u(t), \ldots, R_K^u(t))^T$ and $\mathbf{R}^d(t) = \big(R_1^d(t), \ldots, R_K^d(t)\big)$. The *real-time deployment trajectories* of up and down flexibility reserves are respectively represented by positive vectors $\mathbf{r}_\omega^u(t) = \big(r_{1,\omega}^u(t), \ldots, r_{K,\omega}^u(t)\big)^T$ and $\mathbf{r}_\omega^d(t) = \big(r_{1,\omega}^d(t), \ldots, r_{K,\omega}^d(t)\big)^T$.

In addition, the *real-time up and down flexible ramping trajectories* are respectively represented by vectors $\dot{\mathbf{r}}_\omega^+(t) = \big(\dot{r}_{1,\omega}^+(t), \ldots, \dot{r}_{K,\omega}^+(t)\big)^T$ and $\dot{\mathbf{r}}_\omega^-(t) = \big(\dot{r}_{1,\omega}^-(t), \ldots, \dot{r}_{K,\omega}^-(t)\big)^T$, which are defined as positive and negative components of term $\big(\dot{\mathbf{r}}_\omega^u(t) - \dot{\mathbf{r}}_\omega^d(t)\big)$ in equation (15) of the following problem formulation. Therefore, the proposed flexibility reserve combines the balancing reserve and flexible ramping products in current market practices, as it embeds the up and down flexible ramping trajectories as defined above.

A. The Problem Formulation

The proposed model is formulated as a two-stage stochastic optimization problem. The first stage of the proposed model represents the day-ahead operation where the generation and ramping trajectories and commitment status of generating units are scheduled to supply the mean value of net-load process. The decisions on flexibility reserve capacity trajectories of the units is also made in the first stage. The real-time operation is modeled in the second stage, where the up and down flexibility reserves of generating units and renewable spillage are deployed to compensate the variability and uncertainty of real-time net-load realizations. The proposed stochastic continuous-time UC is formulated in (1)-(16).

$$\begin{aligned}
\min \int_{\mathcal{T}} \Big[& C(\mathbf{G}(t)) + \mathbf{1}^K \big(\mathbf{SU}(t) + \mathbf{SD}(t)\big) \\
& + \mathbf{1}^K \big(\boldsymbol{\mu}^{u,C} \mathbf{R}^u(t) + \boldsymbol{\mu}^{d,C} \mathbf{R}^d(t)\big) \Big] dt \\
& + \int_{\mathcal{T}} \int_{\Omega} \mathbf{1}^K (\boldsymbol{\mu}^{u,E} \mathbf{r}_\omega^u(t) + \boldsymbol{\mu}^{d,E} \mathbf{r}_\omega^d(t)) \mathbb{P}(\omega) dt \; d\omega \\
& + \int_{\mathcal{T}} \int_{\Omega} \mathbf{1}^K (\boldsymbol{\mu}^{+} \dot{\mathbf{r}}_\omega^+(t) + \boldsymbol{\mu}^{-} \dot{\mathbf{r}}_\omega^-(t)) \mathbb{P}(\omega) dt \; d\omega \\
& + \int_{\mathcal{T}} \int_{\Omega} \mu^S SP_\omega(t) \mathbb{P}(\omega) dt \; d\omega, && (1) \\
\text{s.t.} \quad & \mathbf{1}^K \mathbf{G}(t) = D_0(t) - G_0^R(t), && t \in \mathcal{T}, \quad (2) \\
& \mathbf{G}(t) + \mathbf{R}^u(t) \le \overline{\mathbf{G}} \mathbf{I}(t), && t \in \mathcal{T}, \quad (3) \\
& \mathbf{G}(t) - \mathbf{R}^d(t) \ge \underline{\mathbf{G}} \mathbf{I}(t), && t \in \mathcal{T}, \quad (4) \\
& \underline{\dot{\mathbf{G}}} \mathbf{I}(t) + \overline{\dot{\mathbf{G}}}^{SD} \int_{t-\epsilon}^{t+\epsilon} \dot{\mathbf{I}}(t') dt' \le \dot{\mathbf{G}}(t) \\
& \le \overline{\dot{\mathbf{G}}} \mathbf{I}(t) + \overline{\dot{\mathbf{G}}}^{SU} \int_{t-\epsilon}^{t+\epsilon} \dot{\mathbf{I}}(t') dt', && t \in \mathcal{T}, \quad (5) \\
& \mathbf{SU}(t) \ge \mathbf{V} \int_{t-\epsilon}^{t+\epsilon} \dot{\mathbf{I}}(t') dt', \quad \mathbf{SU}(t) \ge 0, && t \in \mathcal{T}, \quad (6) \\
& \mathbf{SD}(t) \ge \mathbf{W} \int_{t-\epsilon}^{t+\epsilon} -\dot{\mathbf{I}}(t') dt', \quad \mathbf{SD}(t) \ge 0, && t \in \mathcal{T}, \quad (7)
\end{aligned}$$

$$\int_{t}^{t+\mathbf{UT}} \mathbf{I}(t')dt' \geq \text{Diag}(\mathbf{UT}) \int_{t-\epsilon}^{t+\epsilon} \dot{\mathbf{I}}(t')dt', \qquad t \in \mathcal{T}, \quad (8)$$

$$\int_{t}^{t+\mathbf{DT}} (\mathbf{1}_K - \mathbf{I}(t'))dt' \geq \text{Diag}(\mathbf{DT}) \int_{t-\epsilon}^{t+\epsilon} -\dot{\mathbf{I}}(t')dt', t \in \mathcal{T} \quad (9)$$

$$\mathbf{1}^K\big(\mathbf{G}(t) + \mathbf{r}^u_\omega(t) - \mathbf{r}^d_\omega(t)\big) = d_\omega(t) - (g^R_\omega(t) - SP_\omega(t)), \qquad \omega \in \Omega, t \in \mathcal{T}, \quad (10)$$

$$-\mathbf{R}^d(t) \leq \mathbf{r}^u_\omega(t) - \mathbf{r}^d_\omega(t) \leq \mathbf{R}^u(t), \ \omega \in \Omega, t \in \mathcal{T}, \quad (11)$$

$$\mathbf{r}^u_\omega(t) \geq \mathbf{0}, \quad \mathbf{r}^d_\omega(t) \geq \mathbf{0}, \qquad \omega \in \Omega, t \in \mathcal{T}, \quad (12)$$

$$0 \leq SP_\omega(t) \leq g^R_\omega(t), \qquad \omega \in \Omega, t \in \mathcal{T}, \quad (13)$$

$$\underline{\dot{\mathbf{G}}}\mathbf{I}(t) + \overline{\dot{\mathbf{G}}}^{SD} \int_{t-\epsilon}^{t+\epsilon} \dot{\mathbf{I}}(t')dt' \leq \dot{\mathbf{G}}(t) + \dot{\mathbf{r}}^u_\omega(t) - \dot{\mathbf{r}}^d_\omega(t) \leq \overline{\dot{\mathbf{G}}}\mathbf{I}(t) + \overline{\dot{\mathbf{G}}}^{SU} \int_{t-\epsilon}^{t+\epsilon} \dot{\mathbf{I}}(t')dt', \qquad \omega \in \Omega, t \in \mathcal{T}, \quad (14)$$

$$\dot{\mathbf{r}}^+_\omega(t) - \dot{\mathbf{r}}^-_\omega(t) = \dot{\mathbf{r}}^u_\omega(t) - \dot{\mathbf{r}}^d_\omega(t), \qquad \omega \in \Omega, t \in \mathcal{T}, \quad (15)$$

$$\dot{\mathbf{r}}^+_\omega(t) \geq \mathbf{0}, \quad \dot{\mathbf{r}}^-_\omega(t) \geq \mathbf{0}, \qquad \omega \in \Omega, t \in \mathcal{T}. \quad (16)$$

The objective of the proposed model, formulated in (1), is to minimize the total cost of first stage decisions and the total expected cost of second stage decisions. The first stage costs are represented in (1) by the first integral over scheduling horizon $\mathcal{T}$, which includes the total generation cost $C(\mathbf{G}(t)) = \sum_{k=1}^{K} C(G_k(t))$ and startup and shutdown costs of units in first line, and the up and down flexibility reserve capacity costs in second line where $\boldsymbol{\mu}^{u,C}$ and $\boldsymbol{\mu}^{d,C}$ are diagonal matrices of up and down flexibility capacity cost coefficients.

The last three lines in (1) represent the second-stage recourse function over scheduling horizon $\mathcal{T}$ and sample space Ω. The third line of (1) formulates the expected cost of deploying up and down flexibility reserve, where $\boldsymbol{\mu}^{u,E}$ and $\boldsymbol{\mu}^{d,E}$ are diagonal matrices of up and down flexibility reserve deployment cost coefficients. The fourth line of (1) formulates the expected cost of deploying up and down flexible ramping, where $\boldsymbol{\mu}^{+}$ and $\boldsymbol{\mu}^{-}$ are diagonal matrices of up and down flexible ramping deployment cost coefficients. The fifth line of (1) formulates the expected cost of renewable spillage, where μ^S is the cost coefficeint of renewable spillage variable $SP_\omega(t)$, and reflects the costs imposed to promote renewable integration and the carbon emission cost avoided by renewable generation [12].

The continuous-time day-ahead power balance constraint (2) schedules the day-ahead generation trajectories of units to supply the expected net-load trajectory of system defined as the mean load trajectory minus the mean renewable generation trajectory, i.e., $D_0(t) - G^R_0(t)$. Constraints (3) and (4) ensure that the generation trajectories plus and minus the up and down flexibility reserve capacities are within capacity limits of the units. The day-ahead ramping trajectories of units are constrained in (5), taking into account the startup and shutdown ramping limits. The startup and shutdown costs are calculated in (6) and (7), where $\mathbf{V}$ and $\mathbf{W}$ are diagonal matrices of startup and shutdown cost parameters. The minimum up and down time constraints are imposed in (8) and (9), where $\mathbf{UT}$ and $\mathbf{DT}$ are the vectors of minimum up and down times. In (5)-(9), $\dot{\mathbf{I}}(t) = (\dot{I}_1(t), \ldots, \dot{I}_K(t))^T$ is time derivative of commitment variables that models the startup and shutdown of the units, where ϵ is an infinitesimally small positive number.

The real-time power balance constraints are presented in (10), where the day-ahead schedule of units, $\mathbf{G}(t)$, stays unchanged and the up and down flexibility reserve and the renewable spillage trajectories are deployed to supply the real-time realizations of net-load, i.e., $d_\omega(t) - g^R_\omega(t)$. The up and down flexibility reserve deployment trajectories are positive variables that are limited in (11) to the capacity trajectories scheduled in first stage. The renewable spillage trajectory is limited in (13) to the renewable generation in each scenario. The ramping constraint (14) ensures that real-time deployment of the up and down flexibility reserves in scenarios would not violate the ramping capability of units. The *up and down flexible ramping trajectories* are defined as positive variables in (15) and (16) as the positive and negative components of the flexibility reserve ramping trajectories of units.

The proposed stochastic continuous-time UC model (1)-(16) is a two-stage stochastic optimizaiton problem with infinite-dimensional decision space in both time and probability sample space, which renders the problem computationally intractable. In the following Sections III and IV, we propose models to reduce the decision space dimension of the problem.

III. Finite-Dimensional Representation of Load and Renewable Generation Processes

The goal here is to reduce the dimensionality of the stochastic processes of load and renewable generation over time, and probability space. In this regard, we first develop a function space model in Section III.A to reduce the dimensionality of the processes over time. The function space model involves modeling the continuous-time mean and realizations of the processes with two different fidelity. In addition, in Section III.B, we develop a second-order moment matching method to reduce the probability spaces dimensionality of the processes.

A. Dimensionality Reduction over Time

A function space model is proposed here to reduce the dimensionality of load and renewable generation processes over time. In the proposed model, we first subdivide the scheduling horizon $\mathcal{T}$ into J intervals $\mathcal{T}_j = [t_j, t_{j+1}), \rightarrow \mathcal{T} = \cup_{j=0}^{J-1} \mathcal{T}_j$, with the same lengths $T_j = T = t_{j+1} - t_j$, and construct a subset of basis functions formed by the Bernstein polynomials of degree Q in each interval $\mathcal{T}_j$, forming a spline function space $\mathbf{e}^{(Q)}(t) = (e^{(Q)}_1(t), \ldots, e^{(Q)}_{(Q+1)J}(t))^T$ to model temporal variations over $\mathcal{T}$, which contains $(Q+1)J$ functions with the following components:

$$e^{(Q)}_{j(Q+1)+q+1}(t) = b_{q,Q}\left(\frac{t - t_j}{T_j}\right), t \in [t_j, t_{j+1}), \qquad (17)$$

for $j = 0, \ldots, J-1; q = 0, \ldots, Q$, where $b_{q,Q}(t)$ is a Bernstein polynomial of degree Q defined as [25]:

$$b_{q,Q}(t) = \binom{Q}{q} t^q (1-t)^{Q-q}, \quad t \in [0, 1). \qquad (18)$$

The function space $\mathbf{e}^{(Q)}(t)$ guarantees the continuity within each interval $\mathcal{T}_j$, but maintaining continuity of trajectories at

interval connection points imposes constraints on the Bernstein coefficients of adjacent intervals, which forms a new reduced-order Bernstein function space $\mathbf{w}^{(Q)}(t) = \mathbf{B}\mathbf{e}^{(Q)}(t)$ with dimension $Z=(Q-1)J+2$, where $\mathbf{B}$ is the mapping matrix. We model the stochastic processes of load, $D(t)$, renewable generation, $G^R(t)$, and the net-load process $N(t)$ on the Bernstein function space $\mathbf{w}^{(Q)}(t)$ as follows:

$$D(t) = \mathrm{D}\mathbf{w}^{(Q)}(t), \qquad \forall t \in \mathcal{T}, \qquad (19)$$

$$G^R(t) = \mathrm{G}^R\mathbf{w}^{(Q)}(t), \qquad \forall t \in \mathcal{T}, \qquad (20)$$

$$N(t) = \mathrm{N}\begin{pmatrix} \mathbf{w}^{(Q)}(t) \\ -\mathbf{w}^{(Q)}(t) \end{pmatrix}, \qquad \forall t \in \mathcal{T}, \qquad (21)$$

where Roman letters D and G^R are Z-dimensional random row vectors, and N is a $2Z$-dimensional random row vector representing Bernstein coefficients of projecting the processes on $\mathbf{w}^{(Q)}(t)$. Hereafter, the degree of a Bernstein function space is used as an indicator of *fidelity* of that function space.

1) Multi-Fidelity Modeling of Mean and Realization Trajectories: the load and renewable generation realization scenarios $D_\omega(t)$ and $G^R_\omega(t)$ are modeled using higher fidelity Bernstein function space Q in (22)-(23), and the mean trajectories $D_0(t)$ and $G^R_0(t)$ using a lower fidelity Bernstein function space of degree $Q' = Q - \alpha$ in (24)-(25):

$$d_\omega(t) = \mathbf{d}_\omega\mathbf{w}^{(Q)}(t), \qquad (22)$$

$$g^R_\omega(t) = \mathbf{g}^R_\omega\mathbf{w}^{(Q)}(t), \qquad (23)$$

$$D_0(t) = \mathbf{D}_0\mathbf{w}^{(Q')}(t) = \mathbf{D}_0\mathbf{M}^\alpha\mathbf{w}^{(Q)}(t), \qquad (24)$$

$$G^R_0(t) = \mathbf{G}^R_0\mathbf{w}^{(Q')}(t) = \mathbf{G}^R_0\mathbf{M}^\alpha\mathbf{w}^{(Q)}(t), \qquad (25)$$

where $\mathbf{d}_\omega$ and $\mathbf{g}^R_\omega$ are Z-dimensional row vectors, $\mathbf{D}_0$ and $\mathbf{G}^R_0$ are $Z'=\big((Q'-1)J+2\big)$-dimensional row vectors of Bernstein coefficients. In (24)-(25), the *degree-raising* property of Bernstein polynomials is utilized to cast the Bernstein coefficients of trajectories, projected on a lower fidelity function space of degree Q', into a higher fidelity function space of degree Q, where $\mathbf{M}^\alpha$ is the $Z' \times Z$ mapping matrix [25].

In addition, we model the realizations $n_\omega(t)$ and mean value $N_0(t)$ of the net-load process respectively in Bernstein function spaces of degree Q and Q', the coefficients of which are related to the respective coefficients of load and renewable generation as follows:

$$\mathbf{n}_\omega = \big(\mathbf{d}_\omega, \mathbf{g}^R_\omega\big), \qquad \mathbf{N}_0 = \big(\mathbf{D}_0\mathbf{M}^\alpha, \mathbf{G}^R_0\mathbf{M}^\alpha\big) \qquad (26)$$

where $\mathbf{N}_0$ and $\mathbf{n}_\omega$ are $2Z$-dimensional row vectors of Bernstein coefficients.

B. Dimensionality Reduction over Probability Space

Here we aim at reducing the probability space dimensionality of load, renewable generation, and the net-load stochastic processes. Assuming a Gaussian process model for $D(t)$, $G^R(t)$ and $N(t)$, the Bernstein random coefficients D, G^R, and N in (19)-(21) would inherit the Gaussian properties of the processes and form a multivariate Gaussian distribution, i.e., $\mathrm{D} \sim \mathcal{N}(\mathbf{D}_0\mathbf{M}^\alpha, \mathbf{K}^d)$, $\mathrm{G}^R \sim \mathcal{N}(\mathbf{G}^R_0\mathbf{M}^\alpha, \mathbf{K}^g)$, $\mathrm{N} \sim \mathcal{N}(\mathbf{N}_0, \mathbf{K}^n)$, where $\mathbf{K}^d$ and $\mathbf{K}^g$ are $Z \times Z$ covariance matrices, and $\mathbf{K}^n$ is a $2Z \times 2Z$ covariance matrix. In Appendix A, given $D_0(t)$, $G^R_0(t)$, $c^d(t,t')$, and $c^g(t,t')$, the derivation of multivariate distributions $\mathrm{D} \sim \mathcal{N}(\mathbf{D}_0\mathbf{M}^\alpha, \mathbf{K}^d)$ and $\mathrm{G}^R \sim \mathcal{N}(\mathbf{G}^R_0\mathbf{M}^\alpha, \mathbf{K}^g)$ is elaborated. Detailed discussion on continuous-time stochastic modeling and estimation of load in Bernstein function space is presented in [26].

We leverage the independence of load and renewable generation processes and write the covariance of the net-load distribution N in terms of the covariance of load and renewable generation distribution as:

$$\mathbf{K}^n = \begin{pmatrix} \mathbf{K}^d & \mathbf{0} \\ \mathbf{0} & \mathbf{K}^g \end{pmatrix}. \qquad (27)$$

The task here is to find the appropriate finite set of S realizations $\hat{\Omega} = \{1, \ldots, \omega, \ldots, S\} \subset \Omega$ that form a representative subset of the infinite-dimensional probability space Ω. To address this, we develop a second-order moment matching method to reduce the dimensionality of the probability spaces. Let $\mathbf{N}^S = (\mathbf{n}_1; \ldots; \mathbf{n}_\omega; \ldots; \mathbf{n}_S)$ be $S \times 2Z$ matrix of Bernstein coefficients of S realizations in $\hat{\Omega}$, and $\boldsymbol{\pi} = (\pi_1, \ldots, \pi_\omega, \ldots, \pi_S)$ be a vector of probabilities. The following Theorem 1 ensures the second-order moment matching between $\hat{\Omega}$ and Ω with minimum of $S = 2Z + 1$ realizations.

Theorem 1. ***Second-Order Moment Matching Dimensionality Reduction:*** *For any S realizations $\mathbf{N}^S$ of* N *with associated probability weights $\boldsymbol{\pi}$ that satisfy the following conditions:*

$$\boldsymbol{\pi}\mathbf{1}^S = 1, \qquad (28)$$

$$\boldsymbol{\pi}\mathbf{N}^S = \mathbf{N}_0, \qquad (29)$$

$$\big(\mathbf{N}^S - \mathbf{1}^S\mathbf{N}_0\big)^T \, Diag(\boldsymbol{\pi}) \, \big(\mathbf{N}^S - \mathbf{1}^S\mathbf{N}_0\big) = \mathbf{K}^n, \qquad (30)$$

the sample space $\hat{\Omega}$ match the first and second moments of $\mathrm{N} \sim \mathcal{N}(\mathbf{N}_0, \mathbf{K}^n)$*, where $\mathbf{1}^S$ is S-dimensional vector of ones.*

Proof: In (28), we ensure that $\boldsymbol{\pi}$ forms a probability measure where its components sum up to 1. Relations (29) and (30) show that the mean and covariance of the realizations match respectively the mean and covariance of $\mathrm{N} \sim \mathcal{N}(\mathbf{N}_0, \mathbf{K}^n)$. These three conditions together ensure the moment matching of order two for min number of realizations $S = 2Z + 1$. ■

In order to calculate the matrix of realizations $\mathbf{N}^S$ and the associated probabilities $\boldsymbol{\pi}$, one needs to solve the system of nonlinear equations (28)-(30). For day-ahead operation with $J = 24$ intervals, this problem includes a very large number of unknowns even for the Bernstein polynomials of low degrees. This procedure would be computationally cumbersome, and the solution convergence highly depends on the choice of initial values. One way to circumvent this problem is to generate second-order moment matching scenarios for the standard uncorrelated Gaussian distribution using the solution offered in [27], and then establish the correlation using the Cholesky decomposition of covariance matrix $\mathbf{K}^n$, as in Theorem 2.

Theorem 2. *Let $\mathbf{L}$ be the Cholesky decomposition of $2Z \times 2Z$ covariance matrix $\mathbf{K}^n$ such that $\mathbf{K}^n = \mathbf{L}^T\mathbf{L}$, and let $\mathbf{H}$ be $S \times 2Z$ matrix of realizations matching the first two moments of standard Gaussian distribution $\mathcal{N}(\mathbf{0}, \mathbf{I})$, and $\boldsymbol{\pi}^{\mathbf{H}}$ be vector of associated probabilities. The realizations calculated as:*

$$\mathbf{N}^S = \mathbf{1}^S\mathbf{N}_0 + \mathbf{H}\mathbf{L}, \qquad (31)$$

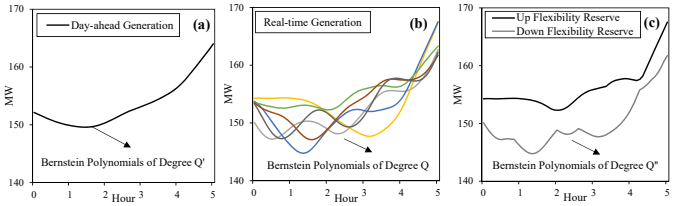

Fig. 1. Fidelity of trajectories: (a) Day-ahead generation trajectory, (b) Real-time generation trajectories associated with net-load realizations, (c) up and down flexibility reserve capacity trajectories.

match the first two moments of $\mathrm{N}\sim\mathcal{N}(\mathbf{N}_0,\mathbf{K}^n)$*, and* $\boldsymbol{\pi}=\boldsymbol{\pi}^{\mathbf{H}}$.

Proof: We seek to establish the relations in Theorem 1 for the realizations defined in (31) and the scenario probabilities $\boldsymbol{\pi}=\boldsymbol{\pi}^{\mathbf{H}}$. Since the scenarios and probabilities in $\mathbf{H}$ and $\boldsymbol{\pi}^{\mathbf{H}}$ match the mean and covariance of the standard Gaussian distribution, then $\boldsymbol{\pi}^{\mathbf{H}}\mathbf{1}^S=1$, $\boldsymbol{\pi}^{\mathbf{H}}\mathbf{H}=\mathbf{0}$, and $\mathbf{H}^T Diag(\boldsymbol{\pi}^{\mathbf{H}})\mathbf{H}=\mathbf{I}$. Since $\boldsymbol{\pi}=\boldsymbol{\pi}^{\mathbf{H}}$, this shows (28). Multiplying (31) by $\boldsymbol{\pi}^{\mathbf{H}}$, we have:

$$\boldsymbol{\pi}^{\mathbf{H}}\mathbf{N}^S=\boldsymbol{\pi}^{\mathbf{H}}\mathbf{1}^S\mathbf{N}_0+\boldsymbol{\pi}^H\mathbf{H}\mathbf{L}=\mathbf{N}_0, \tag{32}$$

which shows (29). Finally, substituting the value of $\mathbf{N}^S-\mathbf{1}^S\mathbf{N}_0$ from (31) in the left hand side of (30), we have:

$$\begin{aligned}\left(\mathbf{N}^S-\mathbf{1}^S\mathbf{N}_0\right)^T Diag(\boldsymbol{\pi})\left(\mathbf{N}^S-\mathbf{1}^S\mathbf{N}_0\right)^T&\\ =(\mathbf{H}\mathbf{L})^T Diag(\boldsymbol{\pi}^H)\mathbf{H}\mathbf{L}&\\ =\mathbf{L}^T\mathbf{H}^T Diag(\boldsymbol{\pi}^H)\mathbf{H}\mathbf{L}&\\ =\mathbf{L}^T\mathbf{I}\mathbf{L}=\mathbf{L}^T\mathbf{L}=\mathbf{K}^n,&\end{aligned} \tag{33}$$

showing (30). This concludes our proof. ∎

IV. Multi-Fidelity Modeling of Decision Trajectories and Operating Constraints

This section develops a reduced-order model for decision variables and constraints of the proposed stochastic UC model (1)-(15). Similar to the ideas in Section III.A, the method in this section is based on reducing the dimensionality of decision trajectories by projecting them in Bernstein function spaces.

The models in this section involve using three Bernstein function spaces with different fidelity to model three sets of decision trajectories, shown in Fig. 1, with different fidelity requirements. The day-ahead generation trajectories of units are modeled with the same fidelity as the day-ahead load and renewable trajectories (Fig. 1-(a)). The real-time deployment trajectories of up and down flexibility reserve and renewable spillage are modeled with the same fidelity as the real-time load and renewable realization trajectories (Fig. 1-(b)). The up and down flexibility reserve capacity trajectories, however, are meant to provide adequate fidelity to follow respectively the up and down uncertainty requirements of net-load, which undergo even faster changes. Thus, the flexibility reserve capacity trajectories of generating units are modeled on a function space of higher fidelity $Q''=Q+\beta$ (Fig. 1-(c)). Details of the proposed multi-fidelity modeling approach are presented next.

A. Modeling the Decision Variables of Generating Units

Here we model the decision variables of generating units in Bernstein function spaces with different fidelity.

1) Modeling Generation Trajectories: day-ahead generation trajectories $\mathbf{G}(t)$ are modeled in the space spanned by $\mathbf{w}^{(Q')}(t)$ as follows:

$$\mathbf{G}(t)=\mathbf{G}\mathbf{w}^{(Q')}(t)=\mathbf{G}\mathbf{M}^{\alpha}\mathbf{w}^{(Q)}(t), \tag{34}$$

where $\mathbf{G}$ is a $K\times Z'$ matrix of projection coefficients.

2) Modeling Flexibility Reserve Trajectories: up and down flexibility reserve *capacity* trajectories $\mathbf{R}^u(t)$ and $\mathbf{R}^d(t)$ are modeled in the space spanned by $\mathbf{w}^{(Q'')}(t)$ as:

$$\mathbf{R}^u(t)=\mathbf{R}^u\mathbf{w}^{(Q'')}(t),\quad \mathbf{R}^d(t)=\mathbf{R}^d\mathbf{w}^{(Q'')}(t), \tag{35}$$

where $\mathbf{R}^u$ and $\mathbf{R}^d$ are $K\times Z''$ matrices of projection coefficients on the function space and $Z''=(Q''-1)J+2$.

Further, the up and down flexibility reserve *deployment* trajectories are modeled in the space spanned by $\mathbf{w}^{(Q)}(t)$ as:

$$\mathbf{r}^u_\omega(t)=\mathbf{r}^u_\omega\mathbf{w}^{(Q)}(t),\quad \mathbf{r}^d_\omega(t)=\mathbf{r}^d_\omega\mathbf{w}^{(Q)}(t),\quad \forall\omega\in\hat{\Omega} \tag{36}$$

where $\mathbf{r}^u_\omega$ and $\mathbf{r}^d_\omega$ are $K\times Z$ matrices of projection coefficients.

3) Modeling the Commitment Status Variables: day-ahead commitment statuses of generating units are projected on the space spanned by $\mathbf{w}^{(Q')}(t)$ as:

$$\mathbf{I}(t)=\mathbf{I}\mathbf{w}^{(Q')}(t), \tag{37}$$

where $\mathbf{I}=(\mathbf{I}_1;\ldots;\mathbf{I}_k;\ldots;\mathbf{I}_K)$ is $K\times Z'$ matrix of projection coefficients. The vector $\mathbf{I}_k=(I_{k,1},\ldots,I_{k,Z'})$ represents the projection coefficients of generating unit k.

4) Modeling the Ramping Trajectories: time derivatives of Bernstein polynomials of a certain degree can be expressed as a linear combination of Bernstein polynomials of smaller degrees [28]. Using this property, day-ahead ramping trajectories are defined in the space spanned by $\mathbf{w}^{(Q'-1)}(t)$ as:

$$\dot{\mathbf{G}}(t)=\mathbf{G}\dot{\mathbf{w}}^{(Q')}(t)=\mathbf{G}\boldsymbol{\mathcal{M}}\mathbf{w}^{(Q'-1)}(t)=\dot{\mathbf{G}}\mathbf{w}^{(Q'-1)}(t), \tag{38}$$

where $\boldsymbol{\mathcal{M}}$ is a $Z'\times(Z'-J)$ matrix relating $\dot{\mathbf{w}}^{(Q')}(t)$ and $\mathbf{w}^{(Q'-1)}(t)$, and $\dot{\mathbf{G}}$ is $K\times(Z'-J)$ matrix of Bernstein coefficients of ramping trajectories, which are linearly related to the Bernstein coefficients of generation trajectories as follows:

$$\dot{\mathbf{G}}=\mathbf{G}\boldsymbol{\mathcal{M}}. \tag{39}$$

Similarly, Bernstein coefficients of the deployment ramping trajectories of flexibility reserves are expressed in terms of Bernstein coefficients of the deployment trajectories as:

$$\dot{\mathbf{r}}^u_\omega=\mathbf{r}^u_\omega\boldsymbol{\mathcal{H}},\quad \dot{\mathbf{r}}^d_\omega=\mathbf{r}^d_\omega\boldsymbol{\mathcal{H}},\quad \omega\in\hat{\Omega}, \tag{40}$$

where $\boldsymbol{\mathcal{H}}$ is a $Z\times(Z-J)$ matrix relating $\dot{\mathbf{w}}^{(Q)}(t)$ and $\mathbf{w}^{(Q-1)}(t)$, and $\dot{\mathbf{r}}^u_\omega$ and $\dot{\mathbf{r}}^d_\omega$ are $K\times(Z-J)$ matrices of Bernstein coefficients. Using (41), constraint (15) can be written in terms of the associated Bernstein coefficients as:

$$\dot{\mathbf{r}}^+_\omega-\dot{\mathbf{r}}^-_\omega=\dot{\mathbf{r}}^u_\omega-\dot{\mathbf{r}}^d_\omega,\quad \dot{\mathbf{r}}^+_\omega,\dot{\mathbf{r}}^-_\omega\geq\mathbf{0},\quad \omega\in\hat{\Omega}, \tag{41}$$

where $\dot{\mathbf{r}}^+_\omega$ and $\dot{\mathbf{r}}^-_\omega$ are $K\times(Z-J)$ matrices of Bernstein coefficients of the up and down flexible ramping trajectories.

B. Modeling the Operation Constraints of Generating Units

1) Generation and Reserve Capacity Constraints: We utilize the convex hull property of Bernstein polynomials to efficiently impose continuous-time inequality constraints. More specifically, the convex hull property states that a trajectory will never be outside of the convex hull formed by Bernstein coefficients of the trajectory [4], [29]. Therefore, the generation capacity constraints (3) and (4), the reserve deployment constraints (11) and (12), and the renewable spillage constraint (13) can be imposed by constraining the associated Bernstein coefficients as follows:

$$\mathbf{G}\mathbf{M}^{\alpha}\mathbf{M}^{\beta}+\mathbf{R}^{u}\leq\overline{\mathbf{G}}\mathbf{I}\mathbf{M}^{\alpha}\mathbf{M}^{\beta}, \tag{42}$$

$$\mathbf{G}\mathbf{M}^{\alpha}\mathbf{M}^{\beta}-\mathbf{R}^{d}\geq\underline{\mathbf{G}}\mathbf{I}\mathbf{M}^{\alpha}\mathbf{M}^{\beta}, \tag{43}$$

$$-\mathbf{R}^{d}\leq\left(\mathbf{r}_{\omega}^{u}-\mathbf{r}_{\omega}^{d}\right)\mathbf{M}^{\beta}\leq\mathbf{R}^{u},\qquad\forall\omega\in\hat{\Omega}, \tag{44}$$

$$\mathbf{r}_{\omega}^{u}\geq\mathbf{0},\quad\mathbf{r}_{\omega}^{d}\geq\mathbf{0},\qquad\forall\omega\in\hat{\Omega}, \tag{45}$$

$$\mathbf{0}\leq\mathbf{SP}_{\omega}\leq\mathbf{g}_{\omega}^{R},\qquad\forall\omega\in\hat{\Omega}, \tag{46}$$

where $\underline{\mathbf{G}}$ and $\overline{\mathbf{G}}$ are $K\times K$ diagonal matrices of minimum and maximum generation capacity limits, $\mathbf{M}^{\beta}$ is a $Z\times Z''$ linear mapping that relates the Bernstein coefficients of degree Q with Bernstein coefficients of degree Q'', and $\mathbf{SP}_{\omega}$ is coefficients row vector of projecting the renewable spillage trajectory $SP_{\omega}(t)$ in the space spanned by $\mathbf{w}^{(Q)}(t)$ defined as:

$$SP_{\omega}(t)=\mathbf{SP}_{\omega}\mathbf{w}^{(Q)}(t). \tag{47}$$

2) Ramping Constraints: Similar to (42)-(46), the convex hull property of Bernstein polynomials is utilized to impose the day-ahead and real-time ramping constraints (5) and (14) by constraining the associated Bernstein coefficients as follows:

$$\underline{\overline{\dot{\mathbf{G}}}}\leq\dot{\mathbf{G}}\leq\overline{\overline{\dot{\mathbf{G}}}}, \tag{48}$$

$$\underline{\overline{\dot{\mathbf{G}}}}\mathbf{M}'^{\alpha}\leq\dot{\mathbf{G}}\mathbf{M}'^{\alpha}+\dot{\mathbf{r}}_{\omega}^{u}-\dot{\mathbf{r}}_{\omega}^{d}\leq\overline{\overline{\dot{\mathbf{G}}}}\mathbf{M}'^{\alpha},\ \forall\omega\in\hat{\Omega}. \tag{49}$$

where $\underline{\overline{\dot{\mathbf{G}}}}$ and $\overline{\overline{\dot{\mathbf{G}}}}$ are $K\times(Z'-J)$ matrices representing respectively the left and right hand side limits of (5) projected on the space spanned by $\mathbf{w}^{(Q'-1)}(t)$, and $\mathbf{M}'^{\alpha}$ is a $(Z'-J)\times(Z-J)$ matrix that relates Bernstein coefficients of degree $Q'-1$ with the Bernstein coefficients of degree $Q-1$. The readers are referred to [4] for details on calculation of $\underline{\overline{\dot{\mathbf{G}}}}$ and $\overline{\overline{\dot{\mathbf{G}}}}$.

3) Startup and Shutdown Cost Constraints: startup and shutdown cost constraints (6)-(7) are reformulated as:

$$SU_{k}(t_{j})\geq V_{k}\left(I_{k}(t_{j})-I_{k}(t_{j-1})\right),\quad j>0,\forall k, \tag{50}$$

$$SD_{k}(t_{j})\geq W_{k}\left(I_{k}(t_{j-1})-I_{k}(t_{j})\right),\quad j>0,\forall k, \tag{51}$$

where V_k and W_k are respectively the startup and shutdown cost parameters of unit k.

4) Minimum Up/Down Time Constraints: minimum up/down time constraints (8)-(9) are reformulated as:

$$\sum_{j'=j}^{j+UT_{k}-1}T_{j}I_{k}(t'_{j})\geq UT_{k}\left(I_{k}(t_{j})-I_{k}(t_{j-1})\right),j>0,\forall k \tag{52}$$

$$\sum_{j'=j}^{j+DT_{k}-1}T_{j}\left(1-I_{k}(t'_{j})\right)\geq DT_{k}\left(I_{k}(t_{j-1})-I_{k}(t_{j})\right),j>0,\forall k, \tag{53}$$

where UT_k and DT_k respectively represent the minimum up and down times of unit k.

C. Modeling Power Balance Constraints

Projecting the day-ahead and real-time decision variables on the spaces spanned by $\mathbf{w}^{(Q')}(t)$ and $\mathbf{w}^{(Q)}(t)$ converts the day-ahead and real-time power balance constraints (2) and (10) into sets of algebraic equations on the associated Bernstein coefficients as follows:

$$\mathbf{1}^{K}\mathbf{G}=\mathbf{D}_{0}-\mathbf{G}_{0}^{R}, \tag{54}$$

$$\mathbf{1}^{K}\left(\mathbf{G}\mathbf{M}^{\alpha}+\mathbf{r}_{\omega}^{u}-\mathbf{r}_{\omega}^{d}\right)=\mathbf{d}_{\omega}-\left(\mathbf{g}_{\omega}^{R}-\mathbf{S}\mathbf{P}_{\omega}\right),\quad\forall\omega\in\hat{\Omega}. \tag{55}$$

D. Modeling the Objective Function

Here we derive the components of objective function (1) in Bernstein function space. Let us consider a prevalent piecewise linear cost function for generating unit k with A_k linear segments of lengths $\overline{g}_{k,1},\ldots,\overline{g}_{k,A_k}$, and associate positive auxiliary variable trajectories $g_{k,n}(t)$ with each of linear segments $n=1,\ldots,A_k$. The linearized generation trajectories and cost functions of units are respectively modeled as:

$$G_{k}(t)=\underline{G}_{k}I_{k}(t)+\sum_{n=1}^{A_{k}}g_{k,n}(t),\ t\in\mathcal{T},\ \forall k, \tag{56}$$

$$\hat{C}\left(G_{k}(t)\right)=C\left(\underline{G}_{k}\right)I_{k}(t)+\sum_{n=1}^{A_{k}}\mu_{k,n}^{g}g_{k,n}(t),t\in\mathcal{T},\forall k, \tag{57}$$

where $\hat{C}\left(G_k(t)\right)$ and $\mu_{k,n}^{g}$ respectively represent the linearized cost function and the slope of linearization segment n. In order to model $\hat{C}\left(G_k(t)\right)$ in Bernstein function space, we expand the auxiliary variables in $\mathbf{w}^{(Q')}(t)$ space as follows:

$$g_{k,n}(t)=\mathbf{g}_{k,n}\mathbf{w}^{(Q')}(t),\ \forall k,\ \forall n, \tag{58}$$

where $\mathbf{g}_{k,n}$ is a Z'-dimensional row vector of Bernstein coefficients, which are constrained to their limits as:

$$\mathbf{0}\leq\mathbf{g}_{k,n}\leq\overline{g}_{k,n}\mathbf{1}^{Z'},\ \forall k,\ n=1,\ldots,A_{k,n}, \tag{59}$$

where $\mathbf{1}^{Z'}$ is a Z'-dimensional row vector of ones. Substituting Bernstein models of $G_k(t)$, $I_k(t)$ and $g_{k,n}(t)$ in (56), Bernstein coefficients of linearized generation trajectory is calculated as:

$$\mathbf{G}_{k}=\underline{G}_{k}\mathbf{I}_{k}+\sum_{n=1}^{A_{k}}\mathbf{g}_{k,n},\quad\forall k, \tag{60}$$

where $\mathbf{G}_k$ is row k of matrix $\mathbf{G}$ defined in (34). Finally, we substitute Bernstein representation of auxiliary variables from (58) in (57), form the linearized total generation cost function as $\hat{\mathbf{C}}\big(G_k(t)\big)=\sum_{k=1}^{K}\hat{C}\big(G_k(t)\big)$, and integrate it over $\mathcal{T}$ as:

$$\begin{aligned}\int_{\mathcal{T}}\hat{\mathbf{C}}\big(G_{k}(t)\big)dt&=\sum_{k=1}^{K}\int_{\mathcal{T}}\Big(C\left(\underline{G}_{k}\right)\mathbf{I}_{k}+\sum_{n=1}^{A_{k}}\mu_{k,n}^{g}\mathbf{g}_{k,n}\Big)\mathbf{w}^{(Q')}(t)dt\\&=\sum_{k=1}^{K}\Big(C\left(\underline{G}_{k}\right)\mathbf{I}_{k}+\sum_{n=1}^{A_{k}}\mu_{k,n}^{g}\mathbf{g}_{k,n}\Big)\int_{\mathcal{T}}\mathbf{w}^{(Q')}(t)dt.\end{aligned} \tag{61}$$

The integral in right hand side of (61) equals to [25]:

$$\int_{\mathcal{T}} \mathbf{w}^{(Q')}(t)dt = \int_{\mathcal{T}} \mathbf{B}'\mathbf{e}^{(Q')}(t)dt = T\frac{\mathbf{B}'\mathbf{1}^{(Q'+1)J}}{Q'+1}, \quad (62)$$

where $\mathbf{B}'$ is the matrix relating $\mathbf{e}^{(Q')}(t)$ and $\mathbf{w}^{(Q')}(t)$, while $\mathbf{1}^{(Q'+1)J}$ is a vector of ones. Substituting (62) in (61), the generation cost is calculated as:

$$\int_{\mathcal{T}} \hat{\mathbf{C}}\big(G_k(t)\big)dt = T\sum_{k=1}^{K}\sum_{j=0}^{J-1} C\left(\underline{G}_k\right) I_k(t_j) + T\sum_{k=1}^{K} \frac{\big(\sum_{n=1}^{A_k} \mu^g_{k,n}\mathbf{g}_{k,n}\big)(\mathbf{B}'\mathbf{1}^{(Q'+1)J})}{Q'+1}. \quad (63)$$

The flexibility reserve capacity cost in line 2 of (1) is calculated as:

$$\begin{aligned}&\int_{\mathcal{T}} \mathbf{1}^K \left(\boldsymbol{\mu}^{u,C}\mathbf{R}^u(t) + \boldsymbol{\mu}^{d,C}\mathbf{R}^d(t)\right) dt \\ &= \mathbf{1}^K \left(\boldsymbol{\mu}^{u,C}\mathbf{R}^u + \boldsymbol{\mu}^{d,C}\mathbf{R}^d\right) \int_{\mathcal{T}} \mathbf{e}^{(Q'')}(t)dt \\ &= T\frac{\mathbf{1}^K \left(\boldsymbol{\mu}^{u,C}\mathbf{R}^u + \boldsymbol{\mu}^{d,C}\mathbf{R}^d\right)(\mathbf{B}''\mathbf{1}^{(Q''+1)J})}{Q''+1} \end{aligned} \quad (64)$$

where $\mathbf{B}''$ is the matrix relating $\mathbf{e}^{(Q'')}(t)$ and $\mathbf{w}^{(Q'')}(t)$. The flexibility reserve deployment cost, flexible ramping cost, and renewable spillage cost in lines 3-5 of (1) are also calculated in a similar way. The function space representation of the objective function (1) is, therefore, calculated as follows:

$$\begin{aligned} &T\sum_{k=1}^{K}\sum_{j=0}^{J-1} \left(C\left(\underline{G}_k\right) I_k(t_j) + SU_k(t_j) + SD_k(t_j)\right) \\ &+ T\sum_{k=1}^{K} \frac{\big(\sum_{n=1}^{A_k} \mu^g_{k,n}\mathbf{g}_{k,n}\big)(\mathbf{B}'\mathbf{1}^{(Q'+1)J})}{Q'+1} \\ &+ T\frac{\mathbf{1}^K \left(\boldsymbol{\mu}^{u,C}\mathbf{R}^u + \boldsymbol{\mu}^{d,C}\mathbf{R}^d\right)(\mathbf{B}''\mathbf{1}^{(Q''+1)J})}{Q''+1} \\ &+ T\sum_{\omega\in\hat{\Omega}} \pi_\omega \frac{\mathbf{1}^K(\boldsymbol{\mu}^{u,E}\mathbf{r}^u_\omega + \boldsymbol{\mu}^{d,E}\mathbf{r}^d_\omega)(\mathbf{B}\mathbf{1}^{(Q+1)J})}{Q+1} \\ &+ T\sum_{\omega\in\hat{\Omega}} \pi_\omega \frac{\mathbf{1}^K(\boldsymbol{\mu}^{+}\dot{\mathbf{r}}^{+}_\omega + \boldsymbol{\mu}^{-}\dot{\mathbf{r}}^{-}_\omega)(\dot{\mathbf{B}}\mathbf{1}^{QJ})}{Q} \\ &+ T\sum_{\omega\in\hat{\Omega}} \pi_\omega \frac{(\mu^S\mathbf{SP})(\mathbf{B}\mathbf{1}^{(Q+1)J})}{Q+1}, \end{aligned} \quad (65)$$

where $\dot{\mathbf{B}}$ is the matrix relating $\mathbf{e}^{(Q-1)}(t)$ and $\mathbf{w}^{(Q-1)}(t)$.

V. Numerical Studies

In this section, the proposed multi-fidelity stochastic UC model is implemented on the IEEE-RTS, using the data given in [30], and the results are provided and compared for multiple studies. The up/down flexibility reserve capacity and deployment costs of units are assumed to be respectively 0.4 and 1.3 times their highest incremental cost given in [30].

Three cases are studied with increasing levels of fidelity for modeling load, solar, generation, reserve capacity and deployment trajectories, as specified in Table I in terms of Bernstein polynomials of degrees Q, Q' and Q''. Note that Case 1 represents the discrete-time stochastic UC model in [12]. We leverage our work in [26] and estimate Gaussian processes for load and solar generation for the three cases, where 5-min CAISO load data of three consecutive Tuesdays from Dec. 5 to Dec. 19, 2017 [31] are used as training data to characterize the load process at Dec. 26, 2017, while the 5-minute CAISO solar power data of three nearest days to Dec. 26, 2017 [31] with similar weather conditions to the day of interest, are utilized as training data for the solar generation predictor. The probability space dimensionality of the estimated processes in three cases is reduced using the moment-matching method developed in Section III, and a total of thirty load and solar generation scenarios are utilized for each case after backward scenario reduction [32]. The results are presented next.

TABLE I
Bernstein Polynomial Degrees of Trajectories in Study Cases

Trajectory	Day-ahead Load, Solar, and Generation (Q')	Day-ahead Reserve Capacity (Q'')	Real-time Load, Solar, and Reserve Deployment (Q)
Case 1	0	0	0
Case 2	3	6	3
Case 3	3	8	6

A. Results

1) System Operation Cost: The first-stage and second-stage costs of the proposed model that represent the day-ahead and expected real-time operation costs are provided in Table II for three cases. The total day-ahead operation cost is comparable for Cases 1 and 3 while it is slightly less for Case 2. However, the sum of day-ahead start-up and energy costs declines from Case 1 to Case 3. The expected real-time operation cost also decreases from Case 1 to Case 3. Note that the flexibility reserve capacity cost increases from Case 1 to Case 3 as we increase the modeling fidelity of trajectories, while the flexibility reserve deployment cost decreases for the cases.

2) Flexibility Reserve Schedule: The aggregate up and down flexibility reserve capacities provided by the units, as well as the envelope of solar spillage trajectories in the scenarios are shown in Figs. 2, where the fine gray trajectories represent the real-time net-load deviation scenarios. In Figs. 2, the positive real-time net-load deviation is compensated by deploying up flexibility reserve, but the negative part is compensated by either deploying down flexibility reserve or solar generation spillage. In the latter, deploying down flexibility reserve not only imposes expected real-time deployment cost but also requires purchasing the associated capacity in day-ahead. However, solar spillage only imposes expected real-time spillage cost. The proposed model would optimize the most economic portfolio of the alternatives to supply the real-time net-load deviation in each scenario. As clear in Fig. 2-(b) and (c), Cases 2 and 3, with higher fidelity trajectory modeling and probability space quantification, capture more variability and uncertainty of net-load as compared to the lower fidelity

TABLE II
OPERATION COST COMPONENTS OF THE PROPOSED STOCHASTIC MODEL

		Case1	Case2	Case3
First Stage (day-ahead) Operation Cost ($)	Start-up Cost	3,610.0	5,083.2	4,866.8
	Energy Cost	378,537.3	372,483.7	372,340.1
	Up Flexibility Reserve Capacity Cost	9,417.1	11,295.4	14,616.6
	Down Flexibility Reserve Capacity Cost	8,106.1	8,796.4	8,535.9
	Total Day-ahead Cost	**399,670.5**	**397,658.6**	**400,359.4**
Second Stage (expected real-time) Operation Cost ($)	Up Flexibility Reserve Deployment Cost	7,481.7	6,628.3	5,506.4
	Down Flexibility Reserve Deployment Cost	6,929.8	6,198.4	4,647.6
	Spillage Cost	112.5	1,069.4	1,462.0
	Total Expected Real-time Cost	**14,523.9**	**13,896.2**	**11,616.0**
Total Operation Cost ($)		**414,194.4**	**411,554.8**	**411,975.4**

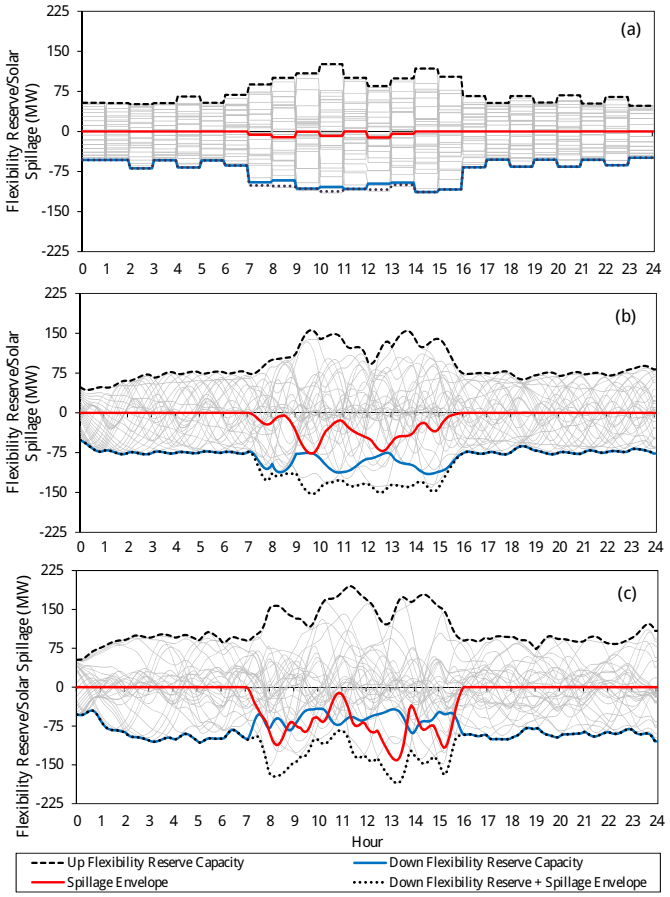

Fig. 2. Flexibility reserve capacity and solar spillage envelope: a) Case 1, b) Case 2, c) Case 3

model in Case 1, which results in higher reserved capacity scheduled in the cases. Quantifying the uncertainty coverage in terms of the area between the reserved capacities, Cases 2 and 3 cover respectively 21.1% and 44.5% more uncertainty as compared to Case 1, while saving respectively $\$2,639.6$ and $\$2,219.0$ in total operation cost in Table II.

3) Flexible Ramping Trajectories: total flexible ramping trajectories provided by the units in each scenario are shown by fine gray trajectories in Figs. 3-(a) and (b) for Cases 2 and

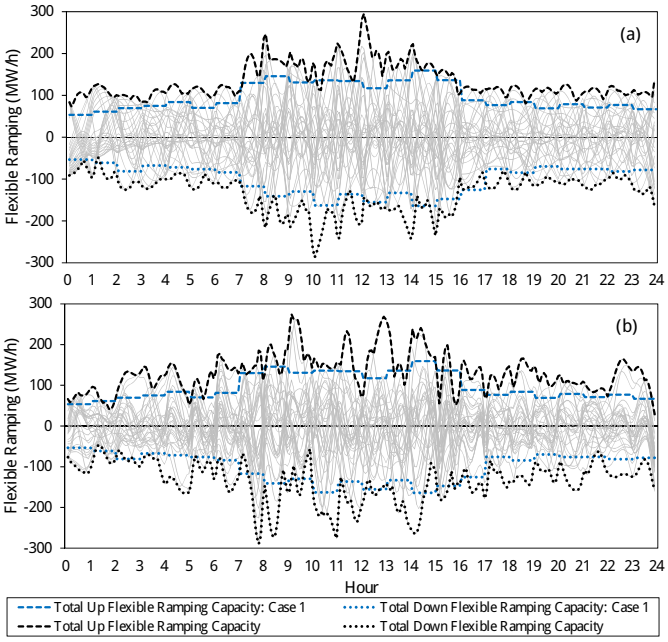

Fig. 3. Flexible ramping capacity: a) Case 2, b) Case 3

3. In Figs. 3, up and down flexible ramping capacities, shown with dashed and dotted black lines, represent the upper and lower envelopes of total flexible ramping trajectories provided by the units in all scenarios. An analogous approach is also adopted for the discrete-time model in Case 1, where the upper and lower envelopes of finite difference of hourly flexibility reserve deployment values (shown by the blue lines in Figs. 3) represent the up and down flexible ramping capacities. As clearly shown in Figs. 3, Cases 2 and 3 secure higher amounts of ramping capacity, scheduled in higher fidelity, to supply the real-time ramping requirements of net-load.

4) Real-time Operation Benefits: Here we aim at comparing the real-time operation benefits of the three cases. In this regard, we generate 10 real-time net-load realizations using the estimated stochastic processes of load and solar generation, and simulate the real-time operation for each realization by solving 288 five-min real-time economic dispatch, considering a ramping scarcity price of $120 per MWh and the day-ahead generation and flexibility reserve schedules of the cases as input parameters. The average values of real-time operation cost components are provided in Table III. In Table III, higher fidelity models in Cases 2 and 3 exhibit lower ramping scarcity, solar spillage, and real-time operation costs. This demonstrate that the proposed multi-fidelity stochastic optimization model schedules a flexibility reserve capacity that more accurately matches the real-time energy imbalance and ramping requirements of net-load.

B. Computation Time

The study cases were solved using CPLEX 12.6.2 [33] on a desktop computer with a 3.6 GHz i7 processor and 64GB of RAM. The computation times to obtain the optimal solution are 4, 33, and 47 minutes for Cases 1 to 3, with an optimality gap of 1%. The computation time of the proposed

TABLE III
AVERAGE REAL-TIME ECONOMIC DISPATCH COST COMPONENTS FOR 10 NET-LOAD REALIZATIONS

	Case 1	Case 2	Case 3
Average Flexibility Reserve Deployment Cost ($)	14,715.1	8,191.4	8,432.9
Average Spillage Cost ($)	20.7	0.0	13.6
Average Flexibility Reserve Scarcity Cost ($)	21,552.8	352.9	0.0
Average Total Cost ($)	36,288.5	8,544.3	8,446.5

model for a given system and a given number of scenarios depends on the fidelity of trajectories. As evidenced in the case studies, increasing the degree of Bernstein polynomials used to model the trajectories not only reduces the day-ahead operation cost of the system in Table II, but also the real-time operation and ramping scarcity costs in Table III. The benefits come at the cost of extra computation time, as the problem size (number of variables and constraints) increases with increasing the degree of Bernstein polynomials. This is, however, an advantage of the proposed model that offers customizable levels of accuracy and computation complexity in approximating the decision space of day-ahead operation problem, which can be tuned by the system operator to match the available time and computational power.

VI. CONCLUSION

This paper presented a stochastic optimization model for multi-fidelity optimization of energy and flexibility reserve in day-ahead power systems operation. The proposed model, formulated as a MILP problem, co-optimizes the day-ahead and real-time operation decisions with different levels of fidelity in a single stochastic optimization problem, which enables capturing and compensating the variability and uncertainty of load and renewable generation that exhibit different levels of variations in day-ahead and real-time operation. The simulation results, conducted on the IEEE-RTS, demonstrate that higher fidelity modeling of day-ahead and expected real-time operation decisions in day-ahead operation results in generation and reserve capacity schedules that more accurately matches the energy and ramping requirements of real-time net-load while saving on total operation cost of the system. Future works include expanding the model to consider transmission constraints, development of a method to determine the optimal degrees of Bernstein function spaces, and investigating options to enhance the computation efficiency of the proposed stochastic optimization model.

APPENDIX A
MULTI-VARIATE GAUSSIAN DISTRIBUTION OF BERNSTEIN RANDOM COEFFCIENTS

Suppose that the mean and covariance of Gaussian load process, $D_0(t)$ and $c^d(t,t')$, are estimated from the historical load data. The mean and covariance of the multi-variate Gaussian distribution of Bernstein random coeffcients, $\mathrm{D} \sim \mathcal{N}(\mathbf{D}_0\mathbf{M}^\alpha, \mathbf{K}^d)$, are linearly related to $D_0(t)$ and $c^d(t,t')$ as:

$$D_0(t) = \mathbf{D}_0\mathbf{M}^\alpha \mathbf{w}^{(Q)}(t),\ t \in \mathcal{T}, \tag{66}$$

$$\begin{aligned} c^d(t,t') &= E[(D(t) - D_0(t))\,(D(t') - D_0(t'))\\ &= \left(\mathbf{w}^{(Q)}(t)\right)^T E[(\mathrm{D} - \mathbf{D}_0\mathbf{M}^\alpha)^T\,(\mathrm{D} - \mathbf{D}_0\mathbf{M}^\alpha)]\mathbf{w}^{(Q)}(t')\\ &= \left(\mathbf{w}^{(Q)}(t)\right)^T \mathbf{K}^d \mathbf{w}^{(Q)}(t'),\quad (t,t') \in (\mathcal{T},\mathcal{T}). \end{aligned} \tag{67}$$

In order to calculate $\mathbf{D}_0\mathbf{M}^\alpha$ and $\mathbf{K}^d$ from (66) and (67), we first choose Z evaluation points $\{t_1,\ldots,t_Z\}$ such that Q points be allocated to the first and last intervals (i.e., $j=0$ and $j=J-1$), and $Q-1$ points be allocated to the rest of intervals. Then we calculate the mean and covariance function $D_0(t)$ and $c^d(t,t')$ at the evaluation points and form respectively the Z-dimensional vector $\mathbf{D}_0(t_s)$ and the $Z \times Z$ matrix $\mathbf{C}^d = [c^d(t_s,t_{s'})],\ s,s' \in \{1,2,\ldots,Z\}$, which are substituted in (66) and (67) forming the following linear set of equations:

$$\mathbf{D}_0(t_s) = \mathbf{D}_0\mathbf{M}^\alpha\mathbf{W}, \tag{68}$$

$$\mathbf{C}^d = \mathbf{W}^T\mathbf{K}^d\mathbf{W}, \tag{69}$$

where $\mathbf{W}=\left(\mathbf{w}^{(Q)}(t_1),\ldots,\mathbf{w}^{(Q)}(t_Z)\right)$ is the matrix of Bernstein basis functions calculated at the evaluation points. The mean vector and covariance matrix of the Bernstein coefficients, $\mathbf{D}_0\mathbf{M}^\alpha$ and $\mathbf{K}^d$, are calculated from (68) and (69) as:

$$\mathbf{D}_0\mathbf{M}^\alpha = \mathbf{D}_0(t_s)\,(\mathbf{W})^{-1}, \tag{70}$$

$$\mathbf{K}^d = \left(\mathbf{W}^T\right)^{-1}\mathbf{C}^d\,(\mathbf{W})^{-1}. \tag{71}$$

Similar derivations apply to random Bernstein coefficients of renewable generation $\mathrm{G}^R \sim \mathcal{N}(\mathbf{G}_0^R\mathbf{M}^\alpha, \mathbf{K}^g)$.

REFERENCES

[1] "Integrating variable renewable energy: Challenges and solutions," 2013, national Renewable Energy Regulatory (NREL), Tech. Rep.

[2] N. Navid and G. Rosenwald, "Ramp capability product design for miso markets," *White paper, July*, 2013.

[3] "Flexible ramping products, revised draft final proposal," California Independent System Operator, 2015.

[4] M. Parvania and A. Scaglione, "Unit commitment with continuous-time generation and ramping trajectory models," *IEEE Trans. Power Systems*, vol. 31, no. 4, pp. 3169–3178, 2016.

[5] G. Angelidis, "Day-ahead market enhancements: Draft technical description," California Independent System Operator, 2018.

[6] E. Lannoye, D. Flynn, and M. O'Malley, "Evaluation of power system flexibility," *IEEE Trans. Power Systems*, vol. 27, no. 2, pp. 922–931, 2012.

[7] ——, "Transmission, variable generation, and power system flexibility," *IEEE Transactions on Power Systems*, vol. 30, no. 1, pp. 57–66, 2015.

[8] M. Huber, D. Dimkova, and T. Hamacher, "Integration of wind and solar power in europe: Assessment of flexibility requirements," *Energy*, vol. 69, pp. 236–246, 2014.

[9] I. G. Marneris, P. N. Biskas, and E. A. Bakirtzis, "An integrated scheduling approach to underpin flexibility in european power systems," *IEEE Trans. Sustainable Energy*, vol. 7, no. 2, pp. 647–657, 2016.

[10] E. A. Bakirtzis, P. N. Biskas, D. P. Labridis, and A. G. Bakirtzis, "Multiple time resolution unit commitment for short-term operations scheduling under high renewable penetration," *IEEE Transactions on Power Systems*, vol. 29, no. 1, pp. 149–159, 2014.

[11] M. Parvania, M. Fotuhi-Firuzabad, F. Aminifar, and A. Abiri-Jahromi, "Reliability-constrained unit commitment using stochastic mixed-integer programming," in *Proc. IEEE 11th International Conference on Probabilistic Methods Applied to Power Systems*, 2010, pp. 200–205.

[12] A. J. Conejo, M. Carrión, and J. M. Morales, *Decision making under uncertainty in electricity markets*. Springer, 2010, vol. 1.

[13] Q. P. Zheng, J. Wang, and A. L. Liu, "Stochastic optimization for unit commitmenta review," *IEEE Trans. Power System*, vol. 30, no. 4, pp. 1913–1924, 2015.
[14] J. Wang, M. Shahidehpour, and Z. Li, "Security-constrained unit commitment with volatile wind power generation," *IEEE Trans. Power Systems*, vol. 23, no. 3, pp. 1319–1327, 2008.
[15] J. M. Morales, A. J. Conejo, and J. Pérez-Ruiz, "Economic valuation of reserves in power systems with high penetration of wind power," *IEEE Trans. Power Systems*, vol. 24, no. 2, pp. 900–910, 2009.
[16] M. Parvania and M. Fotuhi-Firuzabad, "Demand response scheduling by stochastic scuc," *IEEE Trans. Smart Grid*, vol. 1, no. 1, pp. 89–98, 2010.
[17] H. Wu, M. Shahidehpour, A. Alabdulwahab, and A. Abusorrah, "Thermal generation flexibility with ramping costs and demand response in stochastic security-constrained scheduling of variable energy sources," *IEEE Trans. Power Systems*, vol. 30, no. 6, pp. 2955–2964, 2015.
[18] R. Chen, J. Wang, A. Botterud, and H. Sun, "Wind power providing flexible ramp product," *IEEE Transactions on Power Systems*, vol. 32, no. 3, pp. 2049–2061, 2017.
[19] Y. Zhang, J. Wang, B. Zeng, and Z. Hu, "Chance-constrained two-stage unit commitment under uncertain load and wind power output using bilinear benders decomposition," *IEEE Trans. Power Systems*, vol. 32, no. 5, pp. 3637–3647, 2017.
[20] M. G. Fernández-Godino, C. Park, N.-H. Kim, and R. T. Haftka, "Review of multi-fidelity models," *arXiv preprint 1609.07196*, 2016.
[21] N. Chen, Z. Qian, I. T. Nabney, and X. Meng, "Wind power forecasts using gaussian processes and numerical weather prediction," *IEEE Trans. Power Systems*, vol. 29, no. 2, pp. 656–665, 2014.
[22] D. Lee and R. Baldick, "Short-term wind power ensemble prediction based on gaussian processes and neural networks," *IEEE Trans. Smart Grid*, vol. 5, no. 1, pp. 501–510, 2014.
[23] J. Yan, K. Li, E.-W. Bai, J. Deng, and A. M. Foley, "Hybrid probabilistic wind power forecasting using temporally local gaussian process," *IEEE Transactions on Sustainable Energy*, vol. 7, no. 1, pp. 87–95, 2016.
[24] H. Sheng, J. Xiao, Y. Cheng, Q. Ni, and S. Wang, "Short-term solar power forecasting based on weighted gaussian process regression," *IEEE Transactions on Industrial Electronics*, vol. 65, no. 1, pp. 300–308, 2018.
[25] P. M. Prenter *et al.*, *Splines and variational methods*. Courier Corporation, 2008.
[26] R. Khatami, M. Parvania, P. Khargonekar, and A. Narayan, "Continuous-time stochastic modeling and estimation of electricity load," in *Proc. 2018 IEEE Conference on Decision and Control*, 2018, pp. 3988–3993.
[27] D. Xiu, "Numerical integration formulas of degree two," *Applied Numerical Mathematics*, vol. 58, no. 10, pp. 1515–1520, 2008.
[28] P. Dierckx, *Curve and surface fitting with splines*. Oxford University Press, 1995.
[29] M. Parvania and A. Scaglione, "Generation ramping valuation in day-ahead electricity markets," in *Proc. 2016 49th Hawaii International Conference on System Sciences (HICSS)*, 2016, pp. 2335–2344.
[30] R. T. S. T. Force, "The ieee reliability test system-1996," *IEEE Trans. Power Systems*, vol. 14, no. 3, pp. 1010–1020, 1999.
[31] California ISO Operan Access Same-Time Information System, Dec. 2017. [Online]. Available: http://oasis.caiso.com
[32] N. Growe-Kuska, H. Heitsch, and W. Romisch, "Scenario reduction and scenario tree construction for power management problems," in *Proc. IEEE Bologna Power Tech Conference*, June 2003.
[33] The ILOG CPLEX, 2018. [Online]. Available: http://www.ilog.com/products/cplex/

Roohallah Khatami (S' 2015) received B.S. degree from Iran University of Science and Technology, Tehran, Iran, in 2007, and the M.S. degree from Amirkabir University of Technology, Tehran, Iran, in 2013, both in Electrical Engineering. He is working towards Ph.D. degree at the University of Utah. His research interests include power systems operation and electricity markets.

Masood Parvania (SM' 2019) is currently an Assistant Professor of Electrical and Computer Engineering and the Director of Utah Smart Energy Laboratory at the University of Utah. Dr. Parvania serves as an Associate Editor of the IEEE Transactions on Smart Grid and the IEEE Power Engineering Letters, and is the Chair of IEEE PES Utah Chapter, and the Vice-Chair of the IEEE PES Bulk Power Systems Operation Subcommittee and the IEEE PES Risk, Reliability, and Probability Applications Subcommittee. His research interests include the operation, economics and resilience of power and energy systems, and modeling and operation of interdependent critical infrastructures.

Akil Narayan is currently an Assistant Professor at the Department of Mathematics and the Scientific Computing and Imaging Institute at the University of Utah. His research interests are numerical analysis, scientific computing, and uncertainty quantification.